Supporting Information

Self-Enhanced Multifunctional Nanoplatforms for Tumor-Specific Synergistic Therapy *via* NIR-Induced Mild Photothermal and Chemodynamic Effects

Xi Zhang,[a, †] Zhiping Song,[a, †] Yu Han,[a] Jingtong An,[a] Qishan Xu,[a] Xiangyan Chen*[a], Yantao Li*[a]

[a] State Key Laboratory of Advanced Optical Polymer and Manufacturing Technology, Qingdao Key Laboratory of Biomacromolecular Drug Discovery and Development, State Key Laboratory Base of Eco-Chemical Engineering, College of Chemical Engineering, Qingdao University of Science and Technology, Qingdao 266042, China.

Experimental Section

Materials

The following materials were used in this study: Doxorubicin hydrochloride (DOX·HCl, purity >98%), copper chloride ($CuCl_2·2H_2O$), Sodium sulphide ($Na_2S·9H_2O$),sodium hydroxide (NaOH), hydrazine monohydrate ($N_2H_4·H_2O$), polyvinyl pyrrolidone (PVP K30, MW = 40,000), zinc nitrate hexahydrate ($Zn(NO_3)_2·6H_2O$), 2-methylimidazole, Glucose Oxidase (GOX), 5,5'-Dithiobis-(2-nitrobenzoic acid) (DTNB), and 3,3',5,5'-tetramethylbenzidine (TMB) were purchased from Aladdin (China); 4T1 cells (murine breast cancer cells) were purchased from the National Experimental Cell Resource Sharing Platform; Roswell Park Memorial Institute 1640 (RPMI-1640), penicillin-streptomycin solution and phosphate-buffered saline (PBS) were purchased from Pricella; fetal bovine serum (FBS) was purchased from Excell; thiazolyl blue (MTT) was purchased from Macklin (China); dichlorodihydrofluorescein diacetate (DCFH-DA), Calcein AM, and propidium iodide (PI), as well as the reduced glutathione (GSH) content assay kit, were purchased from Solarbio (Beijing, P.R. China); the BCA Protein Assay Kit, adenosine triphosphate (ATP) assay kit, and 2-(4-amidinophenyl)-6-indolecarbamidine dihydrochloride (DAPI) were purchased from Beyotime; Rhodamine 123 (Rh 123) was purchased from MedChemExpress (MCE, Monmouth Junction, NJ, USA). All other chemical reagents and solvents gotten from the suppliers were used without further purification.

Synthesis of HCuS nanoparticles (NPs)

A solution of 100 μL of 0.5 M $CuCl_2$ and 0.24 g of polyvinylpyrrolidone (PVP) was dissolved in 25 mL of deionized (DI) water and stirred at room temperature. Next, 25 mL of NaOH solution (pH=9) was slowly added to the mixture and stirred for 2 min. After that, 6.4 μL of hydrazine solution was added, which led to the formation of Cu_2O spherical particles. Five min later, 200 μL of Na_2S solution (320 mg mL^{-1}) was introduced into the suspension, and the mixture was stirred at 60°C for 2 h. The reaction mixture was then cooled to room temperature, followed by centrifugation (8000 rpm, 10 min) and washing twice with DI water. Finally, HCuS NPs were obtained.

Synthesis of HCuS-DOX NPs

Free doxorubicin (DOX, 0.75 mg mL^{-1}) was mixed with HCuS NPs (1 mg mL^{-1}) in DI water and stirred in the dark for 12 h. The resulting product, HCuS-DOX (HD) NPs, was collected by

centrifugation and washed with DI water. The supernatant was collected, and the absorbance at 480 nm was measured to determine the DOX loading efficiency.

The drug Loading efficiency (LE) and Loading content (LC) were assessed by ultracentrifugation, and the values for LE and LC were calculated as per the following formulas:

$$LE\ (\%) = \frac{Amount\ of\ drug\ encapsulated}{Total\ drug\ \ used} \times\ 100\%$$

$$LC = \frac{Amount\ of\ drug\ loaded}{Total\ nanoparticles}$$

Synthesis of HCuS-DOX@ZIF-8 NPs

A solution of HD (1 mg mL^{-1}) and PVP (20 mg mL^{-1}) in DI water was stirred for 2 h. Then, 2 mL of the PVP-stabilized HD methanol solution was mixed with 4 mL of 2-methylimidazole (2-MIM, 7.125 mg) methanol solution, and the mixture was stirred for 2 min. Subsequently, 4 mL of $Zn(NO_3)_2{\cdot}6H_2O$ methanol solution (15.191 mg) was added to the mixture. After stirring for 30 min, the product, HCuS-DOX@ZIF-8 (HDZ) NPs, was collected by centrifugation (8000 rpm, 10 min).

Synthesis of HCuS-DOX@ZIF-8-GOX NPs

HDZ NPs (1 mg mL^{-1}) were mixed with glucose oxidase (GOX, 0.2 mg mL^{-1}) solution in DI water and stirred for 4 h. The final product, HCuS-DOX@ZIF-8-GOX (HDZG) NPs, was collected by centrifugation, and the supernatant was discarded. The encapsulation efficiency was then measured, and the values for loading efficiency (LE) were calculated using the following formulas:

$$LE\ (\%) = \frac{Amount\ of\ GOX\ encapsulated}{Total\ GOX\ used} \times\ 100\%$$

Characterizations

The zeta potential was analyzed using a Malvern Zetasizer (Nano ZS90, UK). To observe the morphology, transmission electron microscopy (TEM, JEOL JEM-1400, Japan) and scanning electron microscopy (SEM, Zeiss G300, Germany) were conducted. Powder X-ray diffraction (XRD) patterns were recorded on a D/MAX-TTRIII (CBO, Japan). UV-Vis absorbance spectra were recorded with a Shimadzu UV-2600 spectrophotometer (Japan). FTIR spectra were measured on a Bruker FTIR spectrometer (Tensor II, Germany). Fluorescence microscopy was performed using a confocal laser scanning microscope (CLSM, Olympus FV1000, Japan) and an

inverted fluorescence microscope (Nikon Ti, Japan). Protein detection was performed using a Western Blot Imaging System (ImageReader JS-1070P, Peiqing, China).

Photothermal Performance of HDZG NPs

The photothermal efficacy of HDZG was evaluated through infrared thermal imaging to monitor temperature change at different concentrations (0, 50, 100, 200, 400 μg mL^{-1}) under 808 nm laser irradiation (1.0 W cm^{-2}) for 10 min. And the temperature changes of HCHP (200 μg mL^{-1}) were observed within 10 min under different power densities (1, 1.5, 2 W cm^{-2}). The photostability of HDZG NPs was tested by recording the heating and cooling curve during four cycles of 808 nm laser on/off irradiation at 1.0 W cm^{-2}. The PCE of HDZG under 808 nm irradiation at 1.0 W cm^{-2} was determined by measuring the heating and cooling curves of HDZG (200 μg mL^{-1}) and deionized water, with PCE calculated using the specific formula:

$$\eta = \frac{hS\Delta T_{max} - Q_s}{I(1 - 10^{-A})} \quad (1)$$

$$\tau s = \frac{m_D c_D}{hS} \quad (2)$$

$$Qs = \frac{C_D m_D \Delta T_{max2}}{t} \quad (3)$$

In Equation 1, the variable h represents the heat transfer coefficient, while S denotes the surface area of the container. ΔT_{max} refers to the maximum temperature change in the process of heating and cooling. I stands for the power density of the laser, and A represents the absorbance of the solution at a wavelength of 808 nm. Qs represents the heat generated by deionized water under laser irradiation, which can be calculated according to Equation 3. The product of h and S can be obtained by Equation 2, τs represents the time constant of sample and system, $m_D$and c_D denotes the mass and heat capacity of deionized water. In Equation 3, ΔT_{max2} is the maximum temperature difference of deionized water during the heating and cooling process, t representing the duration of the temperature change.

DOX Release Behavior of HDZG NPs *In Vitro*

The standard curve of DOX was established firstly. Drug release experiments were then conducted in phosphate-buffered saline (PBS) at different pH values (pH 7.4 and 5.0).

Typically, 1 mg of HDZG was added to 1 mL of PBS in a tube, followed by shaking at 37°C. For the laser irradiation group, 808 nm laser (1 W cm^{-2}) irradiation was applied for 10 min. At specified time points, the solution was centrifuged, and 1 mL of the supernatant was collected for UV-Vis analysis at 480 nm. The supernatant was then replaced with an equal volume of fresh PBS at the same pH value.

Fenton-like Reactions

To confirm the occurrence of a Fenton-like reaction, 3,3',5,5'-Tetramethylbenzidine (TMB) was employed as a probe to detect the generation of ROS. TMB solution was added to five test tubes, each containing 5 mM glucose: PBS, HCuS, HD, HDZ, HDZG, and HDZG + L808 (1 W cm^{-2}, 10 min). The absorbance of each sample was subsequently measured at 652 nm to assess the Oxidation of TMB.

GSH Depletion Performance of HDZG NPs

A solution was prepared by adding 40 µL of DTNB (10×10^{-3} M) and 100 µL of GSH (10×10^{-3} M) to 760 µL of deionized water, followed by the addition of 100 µL of HDZG. The absorbance at 412 nm was monitored by measuring the solution's absorbance at various time intervals.

Cell Culture Conditions

All cells were maintained in Roswell Park Memorial Institute 1640 (RPMI-1640) supplemented with 1% penicillin-streptomycin and 10% fetal bovine serum (FBS). The cultures were incubated at 37°C in a humidified atmosphere containing 95% air and 5% CO_2.

Cell Uptake

The 4T1 mouse breast cancer cells (1×10^5 cells) were seeded into 24-well plates and allowed to grow until reaching 70-80% confluence. The cells were then incubated with HDZG NPs and free DOX (both containing equivalent concentrations of DOX) at two different time points (1 h and 4 h). Following incubation, cells were washed three times with PBS to remove any unbound drug residues. The cell nuclei were stained using DAPI for 10 min, followed by washing with PBS to remove excess dye. Fluorescent signals were observed under an inverted fluorescence microscope, where red fluorescence indicates intracellular DOX accumulation, and blue fluorescence represents the DAPI-stained nuclei.

Quantitative Analysis of Cellular Uptake

After 1 h and 4 h of incubation, cells were washed with PBS and dissociated using an appropriate solution to collect single-cell suspensions. Fluorescent signals within the cells were quantified using flow cytometry to assess the uptake of HDZG NPs and free DOX by 4T1 cells. FlowJo software was subsequently used to analyze the flow cytometry data, calculating the drug uptake based on the relationship between fluorescence intensity and cell number. This approach enabled precise quantification of drug uptake in cells treated with both HDZG NPs and free DOX.

Cell Viability Assay

4T1 cells were seeded evenly in 96-well plates and cultured 24 h in a CO_2 cell culture incubator. the cells were subjected to various treatments. And the laser groups were subjected to 808 nm laser irradiation (1.0 W cm^{-2}) for 10 min, and incubated for an additional 24 h. Following the treatments, 20 μL of MTT solution was added to each well, and the cells were incubated for 4 h. After incubation, the medium was replaced with 150 μL of DMSO to dissolve the formazan crystals. The optical density (OD) was measured at 492 nm using a microplate reader. Cell viability was calculated using the following formula:

$$Cell\ viability\ (\%) = \frac{OD\ sample}{OD\ control} \times 100\%$$

Cellular GSH Assessment

The 4T1 cells were cultured in 6-well plates and incubated with different treatments. Intracellular GSH levels were assessed using a GSH assay kit. The reaction between DTNB and GSH produced a complex with a distinctive absorption peak at 412 nm. The absorbance value was directly proportional to the GSH concentration.

$$Relative\ GSH\ level = \frac{Absorbance\ of\ experimental\ groups}{Absorbance\ of\ control\ group} \times 100\%$$

ROS Detection and Rh123 Staining

4T1 cells were seeded into 6-well plates and treated with the respective compounds. After 4 h, the cells were stained using appropriate ROS detection and Rh123 staining kits. Following staining, the cells were washed to remove any excess dye, ROS detection was performed using a confocal fluorescence microscope, while fluorescent images of Rh123 were captured using an inverted fluorescence microscope.

Intracellular ·OH Detection

To specifically evaluate intracellular hydroxyl radical (·OH) generation under different

treatment conditions, the ·OH-specific fluorescent probe coumarin-3-carboxylic acid (3-CCA) was employed. The experimental procedure was conducted as follows.

4T1 cells in the logarithmic growth phase were seeded in confocal culture dishes and cultured at 37 °C in a humidified atmosphere containing 5% CO_2 until reaching approximately 70–80% confluence. The cells were then treated with different formulations (Control or HDZG nanoparticles at a concentration of 200 μg mL^{-1}) and incubated for an additional 4 h. After treatment, the culture medium was removed, and the cells were gently washed twice with phosphate-buffered saline (PBS).

Subsequently, the cells were stained with DAPI (1 μg mL^{-1}) to label cell nuclei and incubated at 37 °C for 10 min under dark conditions, followed by three washes with PBS to remove excess dye. The cells were then incubated with serum-free medium containing 3-CCA (final concentration: 12.91 μM) for 30 min in the dark. After incubation, the cells were washed 2–3 times with PBS to eliminate unreacted fluorescent probe.

Finally, fluorescence imaging was performed using an inverted fluorescence microscope. The fluorescence signal generated from the reaction between 3-CCA and ·OH was collected in the blue channel (excitation wavelength ≈ 405 nm, emission wavelength ≈ 450 nm) and used to assess intracellular ·OH production under different treatment conditions.

ATP Content Measurement

4T1 cells were seeded in 6-well plates at a density of 2×10^5 cells/well. After treatment, the culture medium was aspirated, and cells were gently washed twice with PBS. Each well was treated with 200 μL ATP-specific lysis buffer, followed by 20 cycles of pipetting or gentle plate agitation to ensure complete cell lysis. The lysate was centrifuged at 12,000 ×g for 5 min (4°C), and the supernatant was collected for analysis.In a 96-well opaque white plate, 100 μL ATP detection working solution was added to each well and equilibrated for 5 min at room temperature in the dark. Then, 20 μL of sample/ATP standard was added, mixed rapidly with a micropipette, and incubated in the dark for 2 min. Relative luminescence units (RLU) were measured using a chemiluminescence plate reader. Intracellular ATP content was calculated via standard curve fitting.

Western Blot Assay

To assess the expression of HSP 70, When 4T1 cells grown in 6-well plates reached the

appropriate confluence, 4 h of sample treatment, they were lysed and centrifuged to remove debris. Protein concentrations in each sample were quantified using a BCA protein assay kit. The samples were then treated with SDS buffer and boiled for 5 min. Protein samples were separated by SDS-PAGE and transferred to a polyvinylidene fluoride (PVDF) membrane. The membrane was blocked with 5% skim milk in TBST solution, then incubated overnight at 4°C with the primary antibody. After washing with TBST, the membrane was incubated with a secondary antibody for 1.5 h. Protein visualization was performed using a chemiluminescence detection kit.

Live/Dead Cell Staining

To evaluate the cytotoxic effects of nanomaterials on 4T1 cells, cell viability was analyzed using a dual-fluorescence AM/PI staining assay. Specifically, 4T1 cells were seeded in 24-well plates at a density of 1×10^5 cells/well and cultured for 24 h in a 37°C, 5% CO_2 incubator. Cells were then treated with varying concentrations of nanomaterials for 24 h. After treatment, the medium was aspirated, and cells were gently rinsed twice with PBS. Each well was loaded with 500 μL of staining solution containing 2 μM Acetoxymethyl ester (AM, green fluorescence for viable cells) and 2 μM Propidium Iodide (PI, red fluorescence for dead cells), followed by 30 min of incubation in the dark at 37°C. Post-staining, the dye solution was immediately replaced with PBS, and fluorescence images were captured using an inverted fluorescence microscope for viability assessment.

Animals

All animal experiments were performed in compliance with the Institutional Animal Care and Use Committee, and were approved by the Ethics Committee for Animal Experimentation at the Qingdao University of Science and Technology (QKDLL-2024-51). We selected 5-to 6-week-old SPF BALB/c female mice, weighing between 18 and 22 g, obtained from the Ji'nan Pengyue Laboratory Animal Breeding Company. A xenograft tumor model was established by subcutaneously injecting 100 μL of a 1×10^6 cell suspension of 4T1 cells in culture medium. This method was used to establish subcutaneous tumors for subsequent in vivo experiments.

Hemolysis Assay

Fresh mouse blood was collected in an anticoagulant tube, centrifuged to isolate red blood cells, and the supernatant was discarded. The red blood cells were washed with PBS

and diluted to a 1:10 ratio with PBS. The diluted red blood cells were then treated with PBS, deionized water (positive control), and various concentrations of HDZG NPs (0, 50, 100, 200, 400 μg mL^{-1}) at 37°C for 4 h. After treatment, the solution was centrifuged at 3000 rpm, and the 545 nm absorbance of the supernatant was measured.

$$Hemolysis = \frac{(Asample\ -\ Anegative)}{(Apositive\ -\ Anegative)} \times 100\%$$

Thermal Imaging of Tumor Sites In Vivo

After intravenous injection of HDZG NPs (10 mg kg^{-1}) at different times, the tumor site was exposed to an 808 nm laser (1 W cm^{-2}) for 5 min. The photothermal imaging was recorded using an infrared thermal imaging camera.

Anti-Tumor Effects *In Vivo*

Tumor-bearing mice were randomly assigned into five groups once the tumors reached 60-80 mm_3 in size: (1) PBS; (2) HCuS; (3) HCuS+L; (4) HDZG; (5) HDZG+L (10 mg kg^{-1}). Mice were injected via tail vein every two days. Eight hours post-injection, the tumor area of the laser-treated groups was irradiated with an 808 nm laser (1 W cm^{-2}) for 5 min. Body weight and tumor size were recorded every two days.

Tumor volume (V) was calculated using the formula:

$$Volume = \frac{Length\ \times\ Width^2}{2}$$

The TGI rate was calculated using the formula:

$$TGI = (1 - \frac{V_{PBS}}{V_{treatment}}) \times 100\%$$

On day 14, all mice were euthanized. Blood was collected from the orbital sinus for routine blood tests and biochemical analysis. Tumor tissues, as well as heart, liver, spleen, lungs, and kidneys, were dissected and fixed in 4% buffered paraformaldehyde for histological examination.

Statistical Analysis

Data were analyzed using GraphPad Prism (GraphPad Software, CA, USA) and were presented as mean ± standard deviation (SD) from three independent measurements. All microscopy images were processed using ImageJ software. For statistical analysis, a two-tailed Student's t-test was employed to compare two groups, while one-way ANOVA followed by

Tukey's post-hoc test was used for multiple group comparisons. Statistical significance was set at $P < 0.05$.

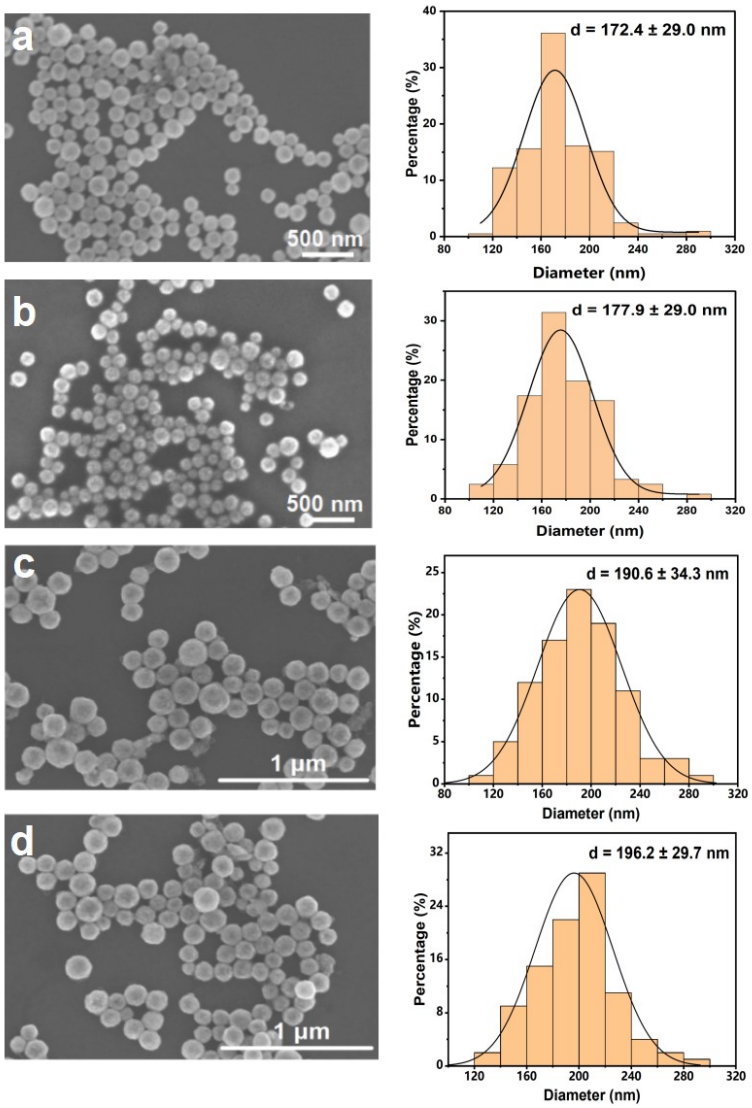

Fig. S1. (a)-(d) SEM images and corresponding statistical particle sizes of HCuS, HD, HDZ, and HDZG NPs.

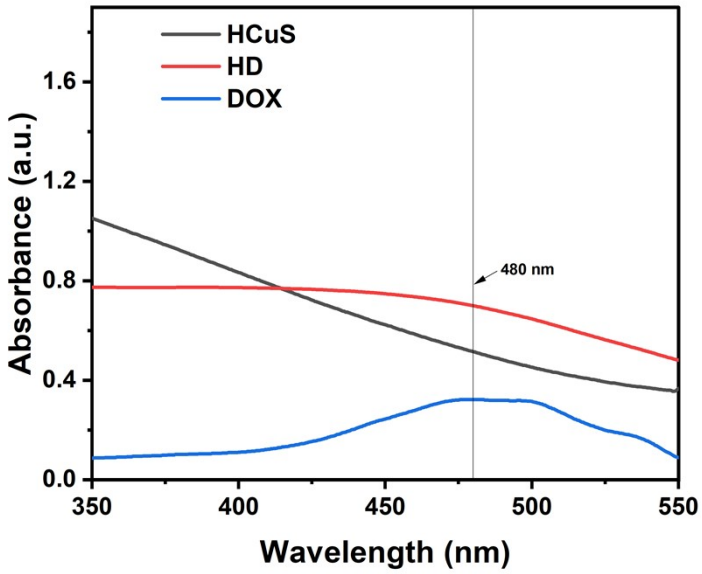

Fig. S2. UV-Vis spectra of HCuS NPs, DOX and HD NPs.

Table S1 Loading efficiency and loading content of DOX molecules in HCuS NPs at different weight ratios.

Weight ratio[a]	Loading efficiency (%)	Loading content[b]
0.1	74.71	0.074
0.25	29.75	0.074
0.5	21.42	0.107
0.75	14.54	0.109
1	7.66	0.076

[a] Weight ratio between DOX and HCuS NPs; [b] Loading content of DOX (mg) in per 1 mg of HCuS NPs.

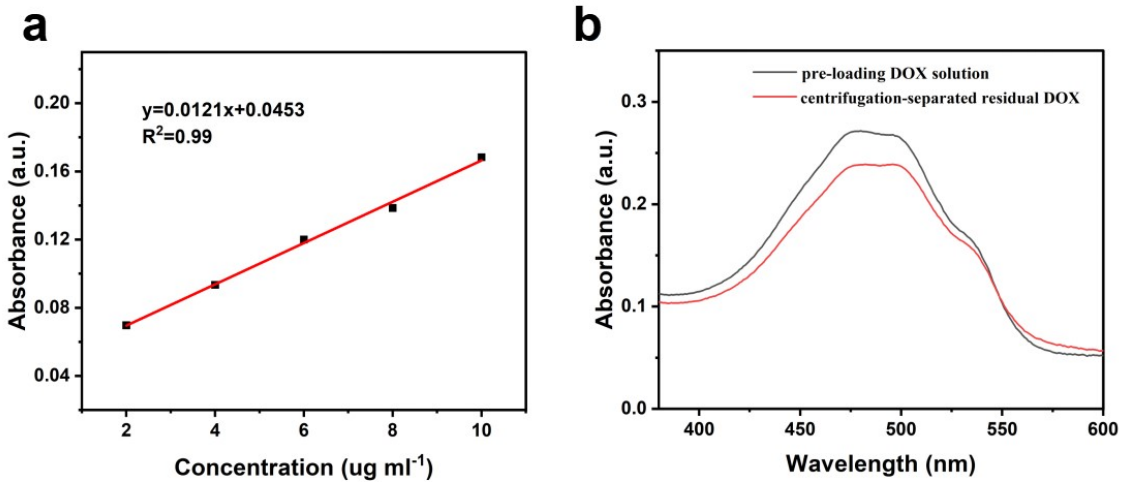

Fig. S3. (a) The standard curve of DOX at different concentrations. (b) The UV-Vis spectra were measured after 40-fold dilution of both the pre-loading DOX solution (before loading into the HD NPs) and the centrifugation-separated residual DOX solution (after removal from the HD NPs by centrifugation), which collectively determined the DOX loading capacity.

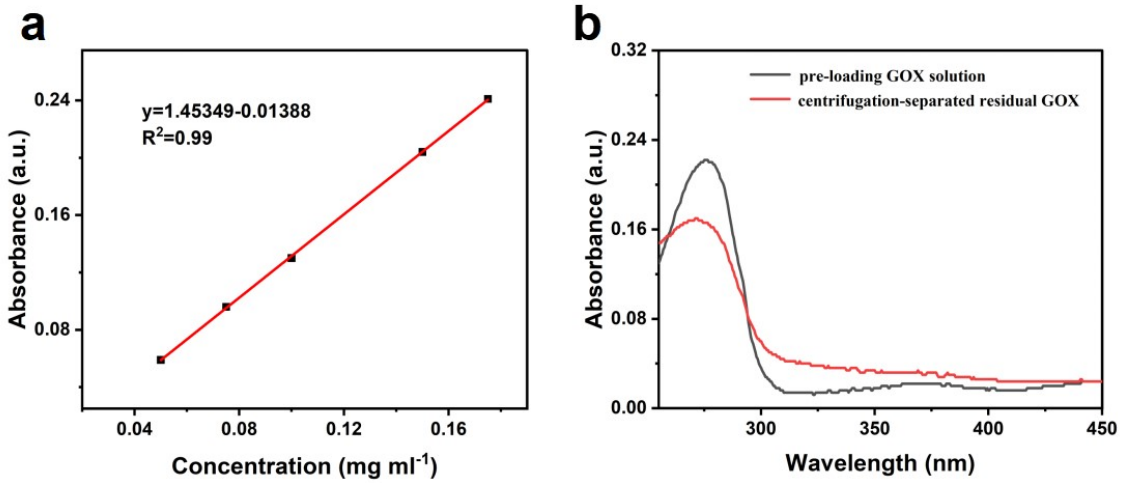

Fig. S4. (a) The standard curve of GOX at various concentrations. (b) UV-Vis spectra of the pre-loading GOX solution (prior to loading into HDZ NPs), and the centrifugation-separated residual GOX (after removing from HDZG NPs by centrifugation).

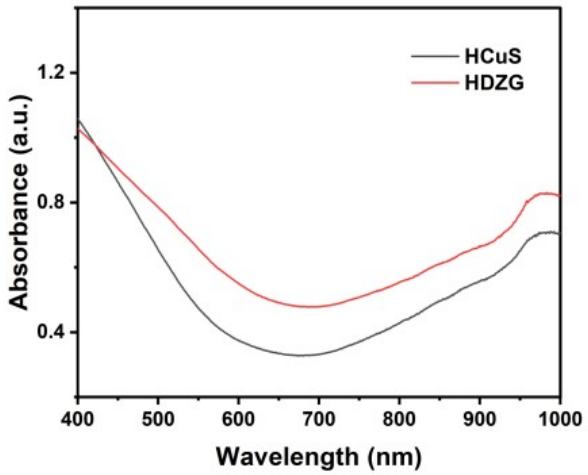

Fig. S5. UV-Vis-NIR absorption spectra of HCuS and HDZG NPs.

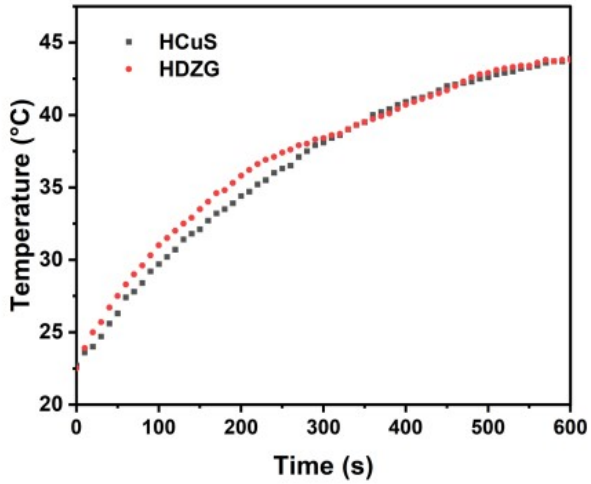

Fig. S6. Temperature curves of HCuS and HDZG NPs at different times under laser irradiation (808 nm, 1W cm^{-2}).

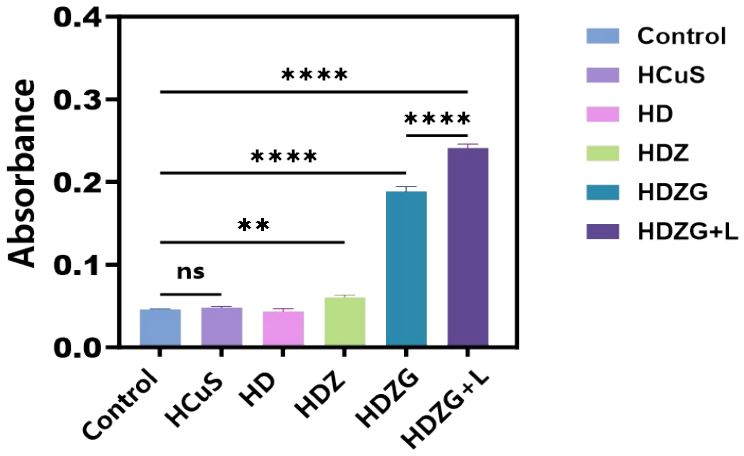

Fig. S7. Quantitative analysis of the UV–vis absorbance of TMB at 652 nm under different treatment conditions in the presence of 5 mM glucose. Data are presented as mean ± SD (n = 3). *P < 0.05, **P < 0.01, ***P < 0.001, **P < 0.0001.

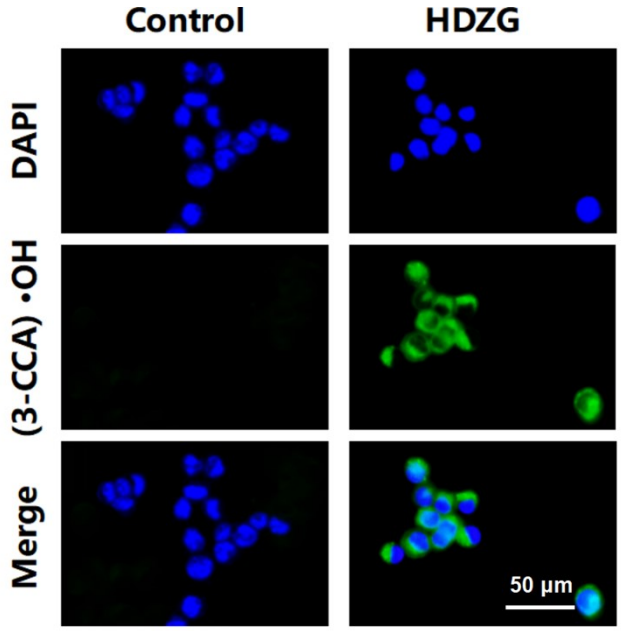

Fig. S8. Intracellular ·OH generation under different treatment conditions evaluated using the fluorescent probe coumarin-3-carboxylic acid (3-CCA).

Confocal laser scanning microscopy was employed to evaluate intracellular ·OH generation using the ·OH-specific fluorescent probe coumarin-3-carboxylic acid (3-CCA). As shown in **Fig. S8**, a markedly enhanced 3-CCA fluorescence signal was observed in HDZG-treated cells, indicating ·OH-associated intracellular ROS generation and supporting the cascade catalytic behavior of the system.

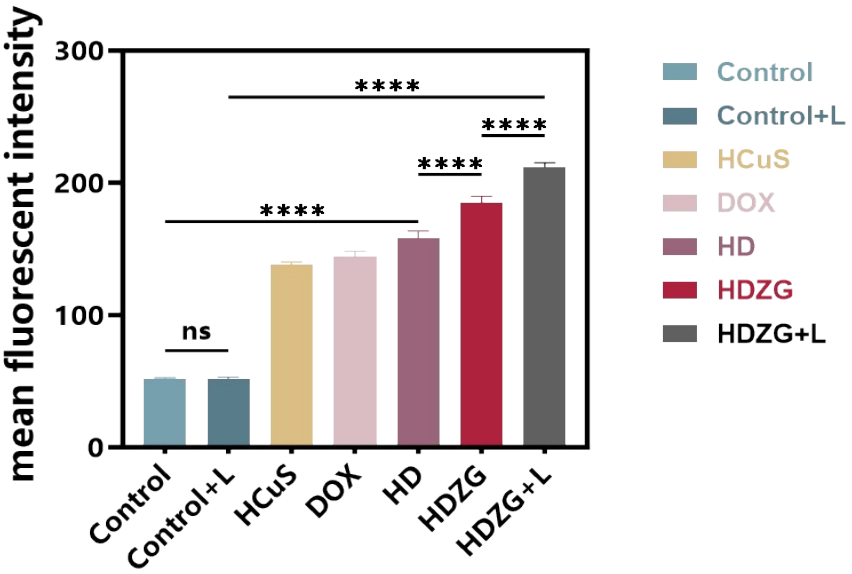

Fig. S9. Quantitative analysis of intracellular ROS levels under different treatment conditions based on fluorescence intensity measured using the DCFH-DA probe. Data are presented as mean ± SD (n = 3). **P* < 0.05, ***P* < 0.01, ****P* < 0.001, ***P* < 0.0001.

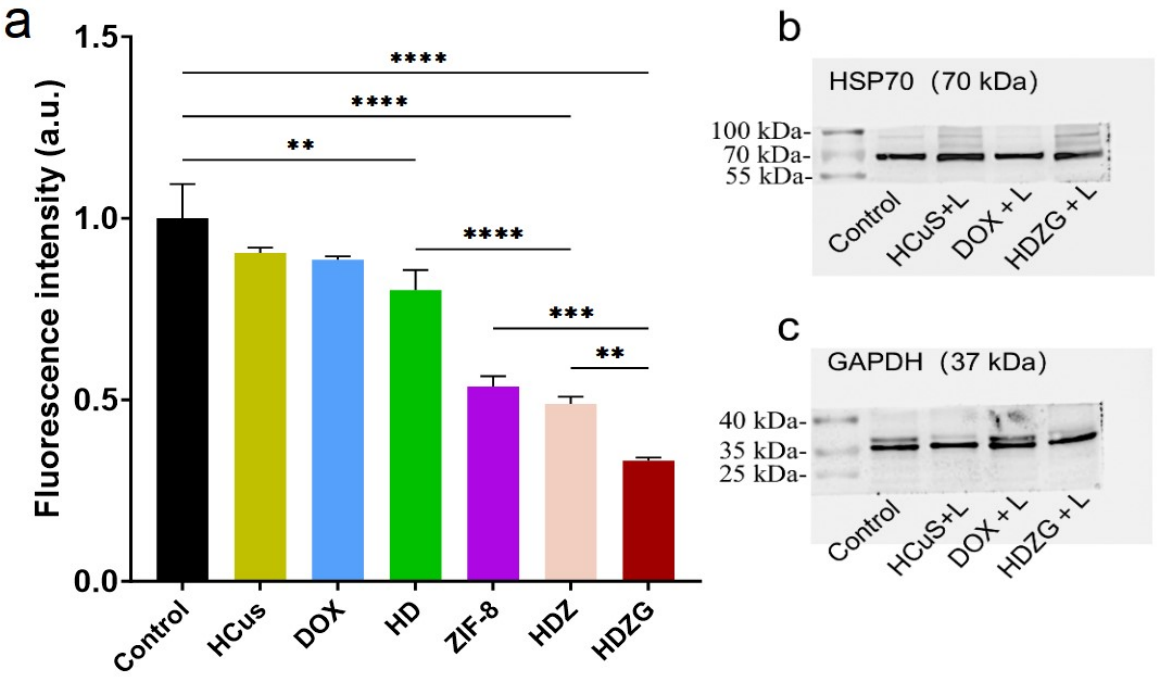

Fig. S10. (a) Semi-quantitative analysis of fluorescence intensity of Rh123 staining. (b) Full-length, uncropped Western blot showing HSP70 expression in 4T1 cells following various treatments. (c) Full-length, uncropped Western blot showing GAPDH expression in 4T1 cells under identical experimental conditions, serving as the internal loading control.

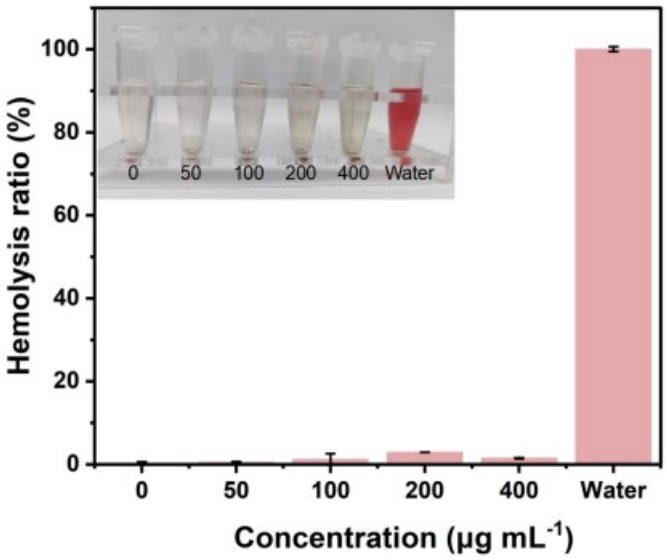

Fig. S11. The hemolysis rates of HDZG NPs under different concentrations. Data were represented as mean ± SD (n = 3).

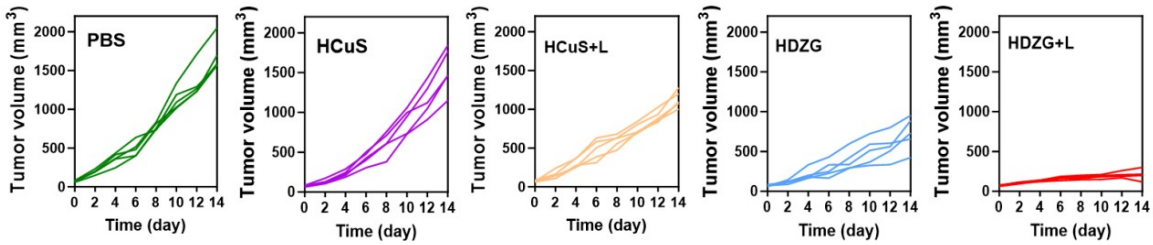

Fig. S12. Individual tumor growth curves in different groups.

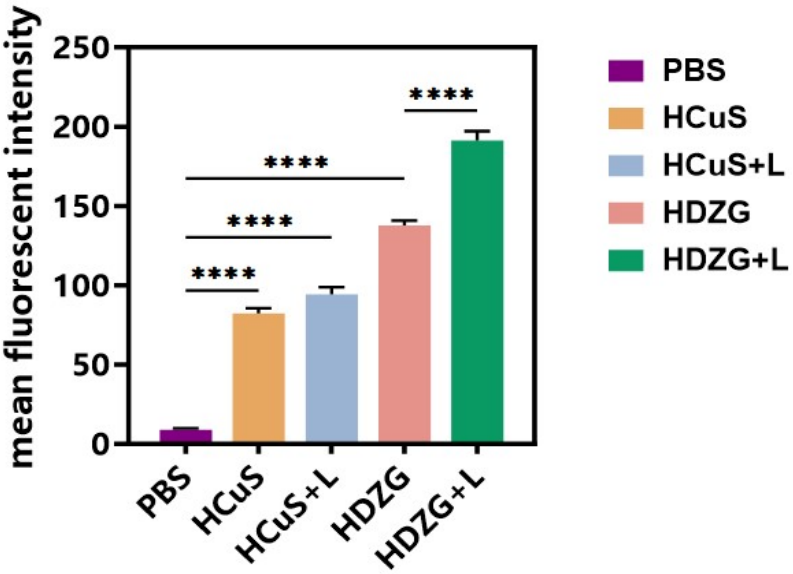

Fig. S13. Quantitative bar plot of ROS immunofluorescence staining in tumor tissues from

tumor-bearing mice under different treatment conditions. ROS-positive signals are shown in red. Data are presented as mean ± SD (n = 5). *P < 0.05, **P < 0.01, ***P < 0.001, **P < 0.0001.

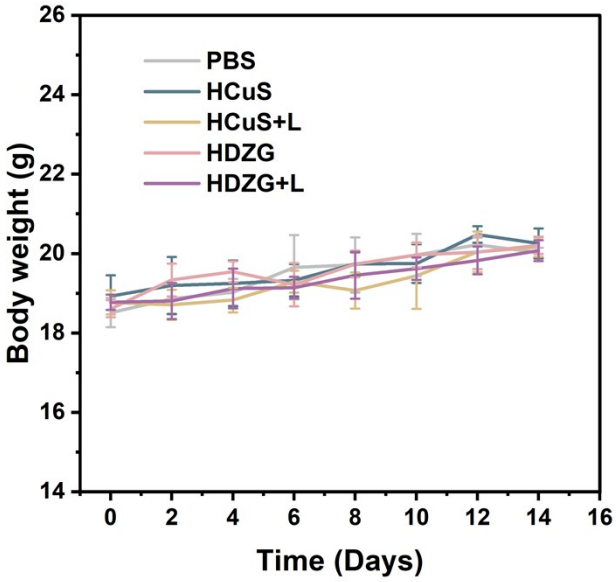

Fig. S14. Body weight monitoring of mice in different treatments. Data were expressed as mean ± SD (n = 5). *P < 0.05, ** P < 0.01, ***P < 0.001, ****P < 0.0001.

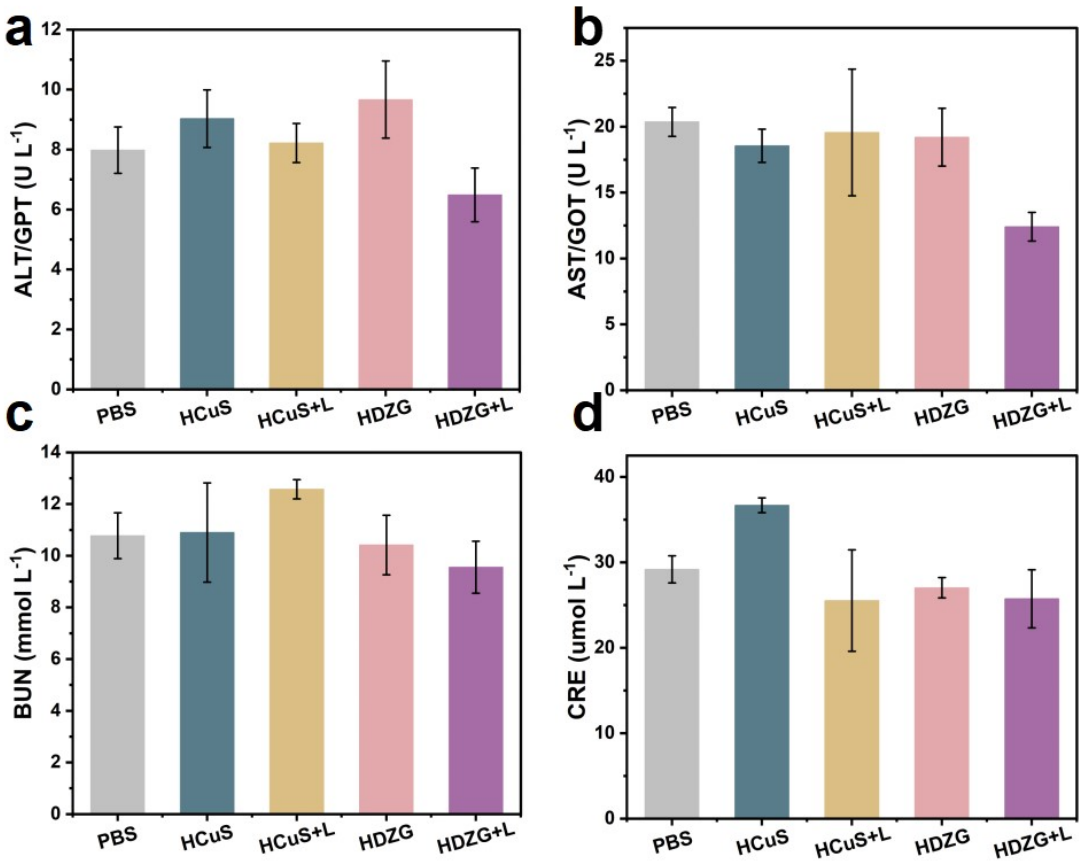

Fig. S15. The expression levels of (a) ALT/GPT, (b) AST/GOT, (c) BUN and (d) CRE in the livers

and kidneys of mice with different treatments. Data were represented as mean ± SD (n = 3).

As shown in **Fig. S15**, although ALT and AST levels in the HDZG + L group are slightly lower than those in other nanoparticle-treated groups, all values remain within a reasonable physiological fluctuation range, with no indication of hepatic injury (*Nature* 2008, 454, 436). Such mild decreases in transaminase levels have been reported in association with reduced tumor burden or alleviated systemic inflammatory stress and are generally not considered adverse biological signals (*ACS Nano.* 2022, 16, 17062).

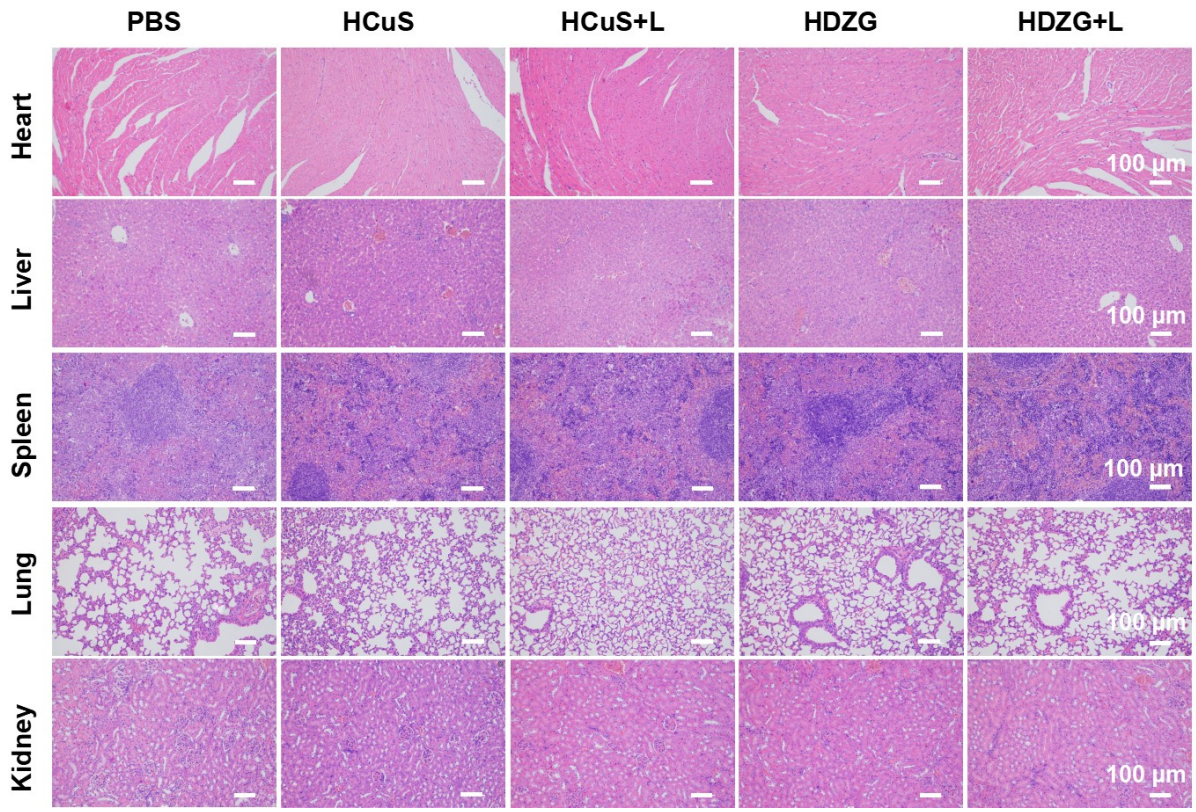

Fig. S16. H&E staining images of major organs obtained from different groups.

As shown in **Fig. S16**, although certain morphological differences (such as spleen) were observed between the treated groups and the PBS control, no obvious pathological features, such as structural disruption, extensive inflammation, hemorrhage, or necrosis, were detected in any major organs. These modest histological variations are therefore considered within normal physiological responses to treatment and nanoparticle biodistribution, indicating good systemic biosafety at the administered dose (*Nanomedicine* 2008, 3, 703).

References

[1] Mantovani, A.; Allavena, P.; Sica, A.; Balkwill, F. Cancer-related inflammation. *Nature*. 2008, 454, 436–444.

[2] Qiu, S.; Wu, X.; Li, Z.; Xu, X.; Wang, J.; Du, Y.; Pan, W.; Huang, R.; Wu, Y.; Yang, Z.; Zhou, Q.; Zhou, B.; Gao, X.; Xu, Y.; Cui, W.; Gao, F.; Geng, D. Biomimetic Magnetosomes as Versatile Artificial Antigen-Presenting Cells for Potent Tumor Immunotherapy. *ACS Nano.* 2022, 16, 17062–17076.

[3] Longmire, M.; Choyke, P. L.; Kobayashi, H. Clearance properties of nano-sized particles. *Nanomedicine.* 2008, 3, 703–717.